IV.   MAGNETOHYDRODYNAMICS OF THE PHOTOSPHERE

SOLAR MAGNETOCONVECTION

Å. Nordlund
Copenhagen University Observatory
Øster Voldgade 3
1350 Copenhagen K
Denmark

R. F. Stein
Dept. of Physics and Astronomy
Michigan State University,
East Lansing, MI 48823
U.S.A.

ABSTRACT.   As a prelude to discussing the interaction of magnetic fields with convection, we first review some general properties of convection in a stratified medium.   Granulation, which is the surface manifestation of the major energy carrying convection scales, is a shallow phenomenon.   Below the surface, the topology changes to one of filamentary cool downdrafts, immersed in a gently ascending isentropic background.   The granular downflows merge into more widely separated downdrafts, on scales of meso-granulation and super-granulation.
   The local topology and time evolution of the small scale, kilo Gauss, network and facular magnetic field elements are controlled by convection on the scale of granulation.   The topology and time evolution of larger scale magnetic field concentrations are controlled by the hierarchical structure of the horizontal components of the large scale velocity field.   In sunspots, the small scale magnetic field structure determines the energy balance, the systematic flows and the waves.   Below the surface, the small scale structure of the magnetic field may change drastically, with little observable effect at the surface.   We discuss results of some recent numerical simulations of sunspot magnetic fields, and some mechanisms that may be relevant in determining the topology of the sub-surface magnetic field. Finally, we discuss the role of active region magnetic fields in the global solar dynamo.

1.   Introduction

With few exceptions (some information from helioseismology measurements), we can only observe the surface manifestations of phenomena in the solar convection zone.   We must deduce by a combination of physical intuition, simple models, and numerical simulations what goes on beneath the solar surface.   The intrinsically three-dimensional nature of flows and magnetic fields in the turbulent solar plasma renders the use of analytical techniques

191

and overly simplified geometries questionable. Rather, we must confront the complex geometries, and use numerical techniques and available computer resources as our tools.

In this review, we summarize recent progress in efforts to understand solar convection and magnetoconvection. In Section 2, we summarize recent results on the topology of solar convection. In Section 3, we report on numerical simulations of sunspot umbrae, and discuss the structure of sunspots below the visible surface. In Section 4, we discuss network and facular magnetic fields, and in Section 5 we briefly discuss the role of active region magnetic fields in the solar dynamo process.

2. Convection Topology

2.1. SURFACE MANIFESTATIONS

Granulation is observationally defined as a well correlated brightness and velocity pattern (e.g. Bray et al. 1984). Some characteristic surface properties are: size scale fractions of *Mm* to a few *Mm*, time scales minutes to half an hour, asymmetry between bright and dark connectivity, asymmetry in the time evolution ("arrow of time"), and a large brightness contrast.

Meso-granulation was first observed as a weak signal in spatially filtered Doppler shift and brightness (November *et al.*, 1981). Its characteristic properties are: size scales of a few *Mm* to 10 *Mm*, time scale hours, horizontal advection of granulation and magnetic fields, weak temperature contrast, weak vertical velocity field. Meso-scale flows are most clearly revealed by auto-correlation tracking of small scale features (granulation) (Title *et al.* 1989, November & Simon 1988), which measures the advection produced by larger scale flows. Meso-scale flows also have noticeable effects on granule growth and on the distribution of granule sizes (cf. the review by Müller 1989, and this volume).

Super-granulation was first observed as a cellular pattern in the horizontal velocity field (Leighton *et al.*, 1962). Its characteristic properties are: size scales of 20 *Mm* to 50 *Mm*, time scale days, organization of the magnetic field into cells, very weak (undetectable) temperature contrast, and very weak vertical velocity field. Super-granular flows are also measurable with the auto-correlation tracking technique. A practical limitation is the size of CCD chips which, together with the resolution required to track individual granules, determines the area coverage.

Observational techniques and limitations (spatial and temporal filters, resolution) often influences the classification into separate phenomena. The original definition of the meso-granulation scale (November *et al.* 1981) was made using spatial filters which excluded smaller and larger scales. The observations demonstrated clearly that "there was something there", but could not accurately address the question of how "well defined" or "separated" the meso-granulation and supergranulation scales are. Simon & Leighton (1964) used a definition of supergranulation size based on the distance to secondary

maxima in auto-correlation spectra. It is not obvious how the distribution of such distances maps onto a distribution of horizontal velocity power as a function of wave number. Simon & Leighton found a broad distribution of distances to secondary maxima, ranging from 20 to 50 *Mm* (cf. their Fig. 4). They adopted as the diameter of supergranulation cells the mean of the secondary maxima measurements, and gave the error as the standard deviation of the mean. This perhaps somewhat arbitrary definition of the size has been quoted ever since as the size of supergranulation cells.

With the autocorrelation tracking technique, it is, in principle, possible to accurately determine power spectra of horizontal velocities, and thus address the question of separation of scales. Since the motions are stochastic in nature, time series which cover a large number of cells, in space and/or time, are necessary to avoid obtaining power spectra which reflect individual cells. For reasons discussed below, it is doubtful on theoretical grounds that there is actually a separation between meso- and super-granulation scales. An observational clarification of this point would be most valuable, and we hope that new observations from La Palma (Scharmer *et al.*, present and future) and SOHO (Scherrer *et al.* 1989) will provide decisive data.

2.2. SURFACE TOPOLOGY: GRANULATION

A qualitative understanding of the granulation phenomenon has emerged from numerical simulations of convection in the surface layers of the Sun (Nordlund 1982, 1983, 1984abc, 1985abcd, Lites *et al.* 1989, Stein & Nordlund 1989) and other stars (Nordlund & Dravins, 1989). One of the main conclusions is that granulation is a shallow *surface phenomenon*, and that the topology below the surface is qualitatively different. To a large extent, the granulation pattern is a manifestation of the interaction of convection with a radiating surface, and the structure of the photosphere is established as a balance between competing convective and radiative processes.

Thermal energy is carried to the surface by advection and released into radiative flux in a thin (50 - 100 *km*) cooling layer. An ascent velocity of some 2 *kms*$^{-1}$ is necessary to sustain the radiative losses at the surface. The photosphere has a stratification which is *strongly sub-adiabatic*; $\Delta \ln T$ (≈ 0.4) $\ll \Delta \ln P \times \nabla_{ad}$ ($\approx 5 \times 0.4 = 2.0$). Thus, unless a significant radiative heating occurred throughout the photosphere, the temperature of the upper photosphere would be much lower. The radiative heating is due to re-absorption of a small, but energetically significant fraction of the radiation, and the detailed temperature structure of the photosphere is the result of a fierce competition between convective (expansion) cooling and radiative heating. As a result, there are large temperature fluctuations on a small scale in the solar photosphere.

Dynamically, the main factors that determine the shape and evolution of the granulation pattern are *advection*, and *buoyancy braking*. The horizontal cellular outflows advect properties (including the flow pattern itself). The result is a tendency for cells to grow horizontally. The competition between neighboring cells in different phases of growth leads to the non-stationary, chaotic evolution of the granular pattern with time. For given vertical

velocities, the horizontal velocities grow linearly with the horizontal size, and thus the pressure fluctuations that drive the horizontal velocities grow quadratically with the horizontal size (cf. Nordlund 1982, Hurlburt *et al*. 1984). This leads to excess densities and hence buoyancy breaking, especially in the centers of large granules which, when otherwise allowed to grow undisturbed, often develop dark centers surrounded by a ring of bright, expanding material ("exploding granules", cf. Bray *et al*. 1984, Section 2.3.7).
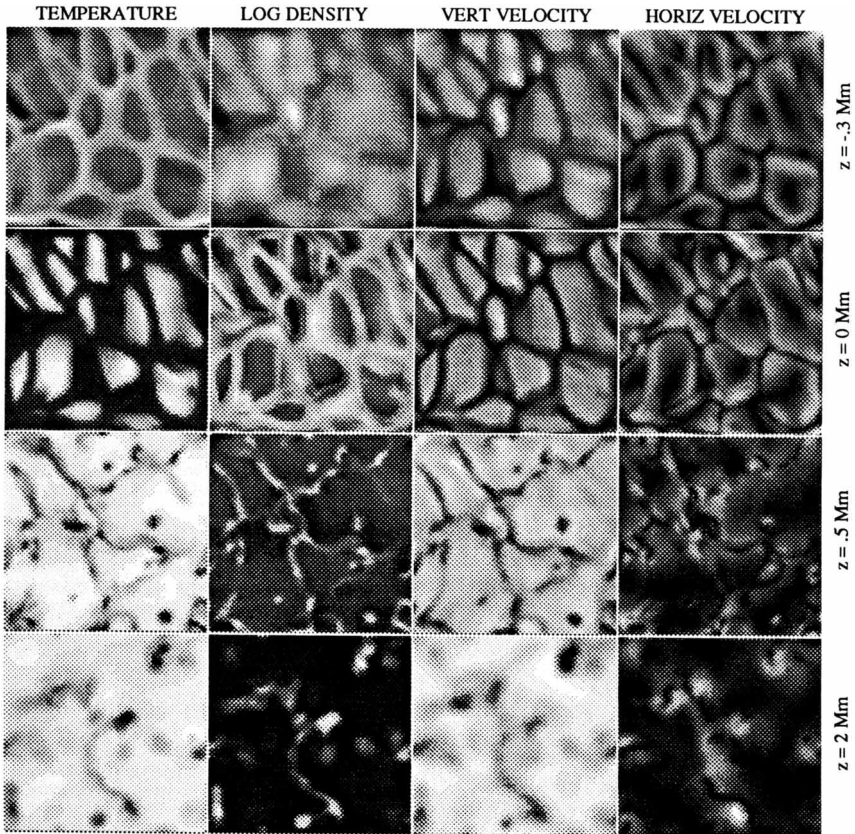

Figure 1. Composite plot, showing temperature, density, and the vertical and horizontal velocity amplitudes in horizontal planes at four different depths in a numerical model of granulation and meso-granulation (Stein & Nordlund, 1989). The horizontal size of the model is 6×6 *Mm*.

2.3. SUBSURFACE TOPOLOGY

Fig 1. illustrates the topology in horizontal planes at, above, and below the surface. Note that below the surface, the horizontal topology changes qualitatively in just a few hundred kilometers. This is a depth interval which is only a fraction of the horizontal cell size. The horizontal topology changes from one with descending gas in connected intergranular lanes to one with isolated spots of descending material. In three dimensions, the topology is *intermittent*, with vertically oriented *filaments* of rapidly descending, entropy deficient material, immersed in a background of slowly ascending, nearly isentropic material. It should be noted that there is no clear cell structure in the vertical direction.

Motions below the surface are nearly adiabatic and anelastic; evolution is mainly by advection. Properties of a fluid element at a given time and place are given by the "sum of the histories" of its constituent parcels. Therefore, test particles are useful in understanding the evolution. Given a record of velocities u(t), particles may be traced forwards and backwards in time. Fig. 2 shows an example of such trace plots.
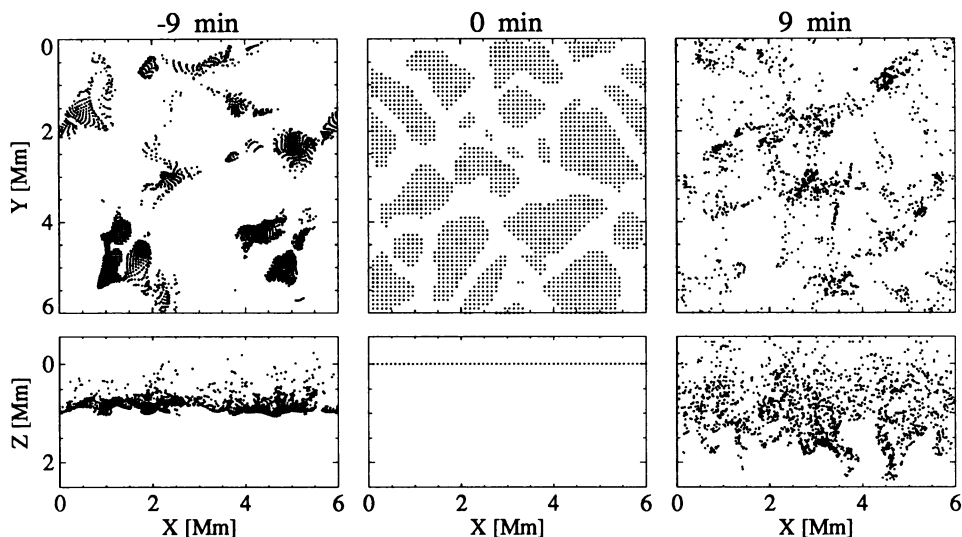

Figure 2. Trace particle plots, showing the location of selected test particles at three different times. The two mid panels show the location at a reference time, with trace particles at all grid points with ascending velocities in the plane $z = 0$. The two panels to the left show the location of these test particles nine minutes earlier, and the two panels to the right show the location nine minutes after the reference time.

As discussed by Stein & Nordlund (1989), the sub-surface topology is a consequence of the density stratification. Because of the strong density

stratification, fluid ascending / descending only a few *Mm* (the size of a cell) must expand / contract orders of magnitude. Because of mass conservation, most *ascending* gas must overturn within a density scale height, while most *descending* gas becomes engulfed in overturning gas, and keeps descending many scale heights. In other words, only a small fraction of the ascending material at any one depth ascends many scale heights, and only a small fraction of the descending material at any one depth overturns within a scale height.

Below the radiating surface, non-adiabatic effects are negligible; the motion is almost *adiabatic*. Furthermore, the rapid expansion of ascending material wipes out entropy inhomogeneities, and thus ascending material is very nearly *isentropic*. Consequently, overturning gas below the surface is also nearly isentropic. This is the reason for the change of topology below the surface; entropy deficient gas in the interconnecting lanes is rapidly replaced with entropy neutral gas below the surface. All entropy deficient material from the surface eventually ends up in the vertices between cells.

It is important to realize that the surface is the only source of entropy fluctuations (except for similar effects at the lower boundary of the convection zone), and thus the surface is also the ultimate cause for the driving of motions.

The fact that the convective flux is directed from the interior towards the surface is perhaps somewhat misleading in this connection; descending cool material and ascending hot material both contribute to a positive convective flux, and because of mass conservation, the ascending and descending mass fluxes are equally large. However, most of the convective flux is carried by the descending filaments, and dynamically the descending filaments are also dominating; most of the kinetic energy density and kinetic energy flux is associated with the descending filaments.

2.4. ANELASTIC MOTION

Below the surface, Eulerian density changes are very small; i.e., the continuity equation acts basically as a *constraint* on the motion; $\partial \ln \rho / \partial t = -\nabla \cdot (\rho \mathbf{u}) \approx 0$. With this *anelastic* form of the continuity equation, the pressure is determined by a Poisson equation and complements the other forces in the equation of motion in such a way as to keep the mass flux divergence free.

Using the Poisson equation for the pressure, one may show that localized (small scale) buoyancy fluctuations lead to localized pressure fluctuations, hence localized motion. On the other hand, large scale buoyancy fluctuations lead to pressure fluctuations who's relative amplitudes vary little with height (cf. Nordlund 1985, Sect. 2.6). In other words, for large scale perturbations, the atmosphere moves locally up/down as a whole, with local stratifications in near hydrostatic equilibrium. As a consequence, large scale components of the horizontal velocity field do not have much vertical shear.

For a horizontally Fourier decomposed velocity field, the anelastic continuity equation implies

$$\frac{u_{\text{vert}}}{u_{\text{hor}}} \approx kH_{\rho u_z} \tag{1}$$

where k is the horizontal wave number, and $H_{\rho u_z}$ is the scale height of the vertical mass flux.

2.5. LARGER SCALE MOTIONS

In the interior of the convection zone, a more gradual change of the topology occurs. The downflows that originate from intergranular lanes at the surface merge into fewer, more widely separated filamentary downdrafts. The horizontal velocities of the large scale flows advect the small scale structure sideways to produce this merging. As a result, the horizontal scale of the velocity field increases with depth. Conversely, it is the merging smaller scale filaments which provide the entropy fluctuations that drive the larger scale flows.

The small density scale height in the surface layers dictates that the energy carrying convection cells (which must have vertical velocities in excess of some 2 kms^{-1}) must not be larger than a few Mm near the surface (cf. Eq. (1) above). At larger depths, larger cell sizes are allowed, and according to the discussion above, larger scales are indeed driven by the merging of smaller scale filaments from the surface layers.

The simulations have demonstrated this only for scales marginally larger than the surface granulation, but presumably the same mechanism works for still larger scales, including the supergranular scale. The general scenario then is one where the merging of downdrafts on granular scales drives flows on meso-granular scales at a depth of a few Mm below the surface, and the merging of meso-granular downdrafts drives flows on supergranular scales at depths of some 10 - 20 Mm. Presumably, flows on even larger scales (traditionally called giant-cells) are driven at even larger depths, by merging supergranular downdrafts.

As mentioned earlier, the pressure fluctuations which drive the horizontal components of large scale velocity fields extend over a height range comparable to or larger than the horizontal size of the fluctuations. Since the aspect ratio (ratio of horizontal size to distance from the surface) of these flows is larger than unity, this implies that the horizontal velocity fields of larger scale flows extend up to the surface. The numerical simulations indicate similar vertical and horizontal rms amplitudes below the surface. Accordingly, the distribution of surface horizontal velocity amplitude with horizontal size reflects the dependence of vertical velocity amplitudes on depth below the surface.

There is no obvious reason why, in this process, certain distinct scales should be favored. The often mentioned helium ionization zones, which extend over quite a range in depth, centered at some 5 and 15 Mm, has no particular relevance in this scenario, except for reducing the adiabatic temperature gradient, and hence somewhat reducing the density scale height.

The effect is a change in the density scale height, but only of a few tens of percent, and is hardly likely to have much effect on the distribution of horizontal velocity amplitude with horizontal size.

2.6. GLOBAL CONVECTION ZONE FLOWS

We expect the strong asymmetry between ascending and descending motions to prevail on all scales, including scales comparable to the depth of the convection zone. The merging downdrafts with entropy deficient gas are likely to extend throughout the convection zone. Turbulence in the downdrafts induces mixing with surrounding, entropy neutral fluid, but because of the general convergence of descending gas, only a small fraction actually turns over into ascending gas. At the very bottom of the convection zone, the downdrafts hit the interface to the stable region below the convection zone. In this layer, descending gas is diverging, ascending gas is converging, and overturning gas is reheated by radiative diffusion or by mixing. The situation is to some extent the reverse of that at the surface. However, at some distance above the lower boundary, ascending gas again must be expanding, and the analogy to the surface layers is lost.

It would seem that the global dynamics of the convection zone must be strongly influenced by the asymmetry between descending and ascending gas, and that models that do not take this asymmetry properly into account may easily fail to produce realistic result. This is a likely cause for the failure of current numerical global convection zone models (Gilman & Miller 1986, Glatzmaier 1987) to predict differential rotation properties and dynamo action consistent with the observations.

The observational evidence (cf. Libbrecht 1988, and other references in the same proceedings) indicates that the differential rotation of the solar convection zone to a first approximation is constant along radii, rather than constant on cylinders (as predicted by the Taylor-Proudman theorem). This shows that, in some sense, the solar convection zone is "vertically stiff"; i.e., ascending and descending material tend to conserve angular speed, rather than angular momentum.

If the topology of the global convection zone is intermittent, with localized filamentary downdrafts immersed in a gently ascending background, then it might be possible to work out simplified models of the differential rotation, where the exchange of angular momentum between ascending and descending flow components is estimated from drag and mass exchange between the filamentary downdrafts and the gently ascending background. As discussed above, the mass exchange between the ascending and descending components is largely determined by the vertical mass flux scale height, through the continuity equation.

3. Magneto-Convection

We now turn our attention to convection in the presence of a magnetic field, starting with the extreme case of sunspot umbrae.

3.1. UMBRAL SIMULATIONS

We have recently performed a preliminary simulation of the central parts of a sunspot umbra (Nordlund & Stein 1989). In this simulation, a vertically homogeneous magnetic field with a strength of 0.2 T (2 kG) is superimposed on a snapshot from a granulation simulation. This adds a constant pressure everywhere in the atmosphere, but produces no additional forces. Hence the initial condition is self-consistent, although somewhat artificial. The strong magnetic field rapidly quenches the convection.
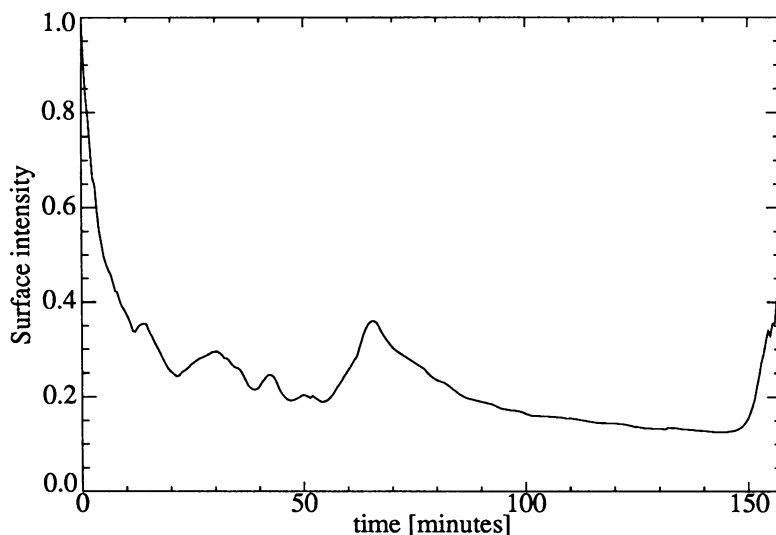

Figure 3. The average surface intensity in an umbra simulation, relative to the initial photospheric surface intensity, as a function of time.

Fig. 3 shows the average surface intensity as a function of time for this simulation. Because convection is suppressed, there is nothing to compensate for the strong radiative losses at the surface, and the surface begins to cool rapidly. Within 5 minutes, the surface radiation intensity is less than half the nominal one. Due to the rapidly decreasing surface flux, and the exponentially increasing heat capacity per unit volume (because the visible surface descends), the rate of cooling slows down, and it takes approximately one hour to reach a surface intensity of 20 %. We regard our initial condition as rather artificial, but the slow cooling, and the formation of a dark umbra "in place", may correspond to a particular umbra formation

process, with no accompanying convergence of pores and small scale magnetic features, observed by Zirin (1987).

Fig. 4 shows the corresponding evolution of the horizontally averaged temperature, as a function of time and depth. The very steep temperature drop near $\tau = 1$ is obvious, and one may follow the descent of this surface as a function of time by noting that the vertical distance between grid lines is approximately 50 km. Note that the $\tau = 1$ surface descends approximately
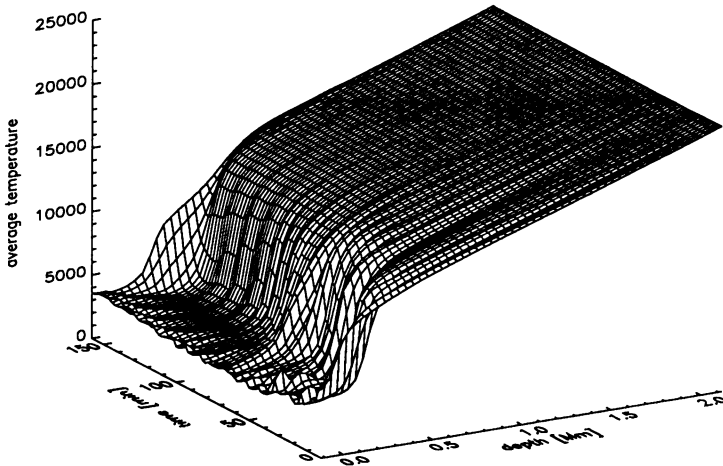

Figure 4. The horizontally averaged temperature in the umbra simulation, as a function of time and depth. The total time covered is about two and a half solar hours. The fine structure in the atmosphere in the first part of the simulation is an artefact of the initial conditions.

400 km in about one hour.

Some of the variation of the surface intensity with time visible in Fig. 3 is due to a vertical buoyancy oscillation that was present in the initial model, and which continues, driven by inertia. However, the two dominant peaks are due to two episodes of convection, which carry heat up to the surface and thus increase the surface radiative flux. Fig. 5 shows the horizontally averaged convective flux, as a function of time and depth. Note that, for brief periods, the convective flux just below the surface exceeds the nominal *photospheric* surface flux. During the first episode, the convective flux peaks at just over 100 % of the nominal solar flux, but during the second episode it exceeds 300 % of the nominal solar flux. The convective flux is localized to a shallow layer centered on the steepest part of the temperature distribution, and serves to slightly flatten the temperature profiles displayed in Fig. 4. This increases the surface temperature and hence the surface radiative flux.

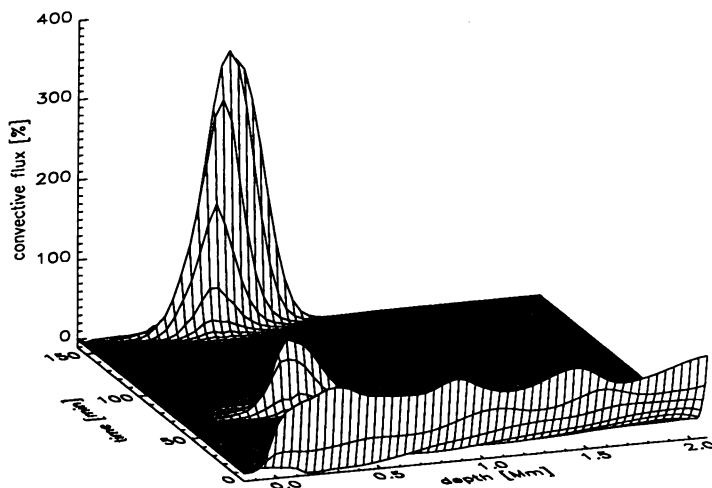The effect on the surface radiative flux is only about 15 % during the

Figure 5. The average convective flux in the umbra simulation, as a function of time and depth. The convective flux that is present in the initial snapshot rapidly dies away. Later, after about one solar hour, and after about two and a half solar hours, short episodes of convection develop in a narrow surface layer.

first episode, which may be surprising considering the convective flux of over 100 % just below the surface. However, the heat capacity of the surface layers is large, and the huge divergence of the convective flux only leads to a rather insignificant flattening of the average temperature profile. During the second episode, the convective flux is large enough - and its duration long enough - to significantly heat the surface layers. This results in an upward displacement of the surface temperature drop, with a corresponding increase in the surface radiation intensity, which reaches about 40 %.

The topology of the heat flow is similar to that of ordinary granulation, with cells of ascending and expanding gas which push the magnetic field aside. The cells are roundish, not space filling, and their size taper off with height, because of the increasing dominance of the magnetic pressure. The surface brightness pattern has bright edges on the round cells, because of the transparency of the plasma in the surrounding, strong magnetic field. As illustrated by Fig. 5, the flow pattern is shallow.

3.2. UMBRAL STRUCTURE

The qualitative features of an umbra's vertical structure may be deduced from simple considerations of pressure and energy equilibrium. To a first approximation, sunspot umbrae are similar to cool stellar atmospheres with inhibited convection. At lower temperatures the opacity is smaller, so the pressure at $\tau = 1$ is larger. Inhibition of convection reduces the convective

heat flux, so the $\tau = 1$ layer is cooled by radiation. Since the convective flux is small, the atmosphere is close to radiative equilibrium, and the temperature rises rapidly below the surface until it reaches the interior adiabat. The bottom of the steep temperature gradient is an important "pivot" (transition) point in the structure of the umbra.

In fact, the "pivot point" may be defined as the place where the radiative flux becomes a small fraction of the surface flux. Above this point, there is approximate radiative equilibrium, because the time scale to approach radiative equilibrium decreases rapidly with height. Near the pivot point, there is a significant divergence of radiative flux, which must be balanced either by the divergence of another (e.g. convective) energy flux, or else by a local loss of thermal energy. In the latter case, the loss of thermal energy implies that the pivot point descends with time. Its rate of descent is determined by the ratio of the surface radiative energy loss to the energy density per unit volume at the pivot point. The pivot point must lie rather close to the visible surface ($\tau = 1$), since the gas rapidly becomes very opaque below the surface. The depth of the pivot point is basically the same as the "Wilson depression"; i.e., the height difference between $\tau = 1$ in the umbra and in the surrounding photosphere. Thus, if there is negligible convective flux in the deep umbra, the umbra surface descends; i.e., the Wilson depression increases with time. If and when convection becomes sufficiently effective to compensate for the surface energy losses, the umra ceases to descend. The vertical position of the umbra at any one time is determined by how long it has been cooling, and how much heat has been replenished by convection. The shape of the temperature profile is qualitatively the same inside and outside the umbra, with a deep, nearly isentropic part, separated from the cool optically thin atmosphere by a steep temperature drop just below the visible surface.

In the external photosphere, the isentropic region extends all the way up to just below the surface of the photosphere. Inside the umbra the visible surface and steep temperature gradient are depressed, as discussed above. Thus, there is a depth interval between the surface of the photosphere and the surface of the umbra where the temperature inside the spot is much smaller than the temperature in the surrounding photosphere. As a consequence, the internal gas pressure drops much more rapidly with height in this interval than the external gas pressure. The gas pressure difference, which controls the strength and topology of the magnetic field at the edge of the spot, thus obtains a characteristic shape. From its small subsurface value, the difference increases rapidly with height near the pivot point, because of the drop in the interior temperature. When the internal gas pressure is negligible compared to the external pressure, the pressure difference is essentially equal to the external pressure, and hence decreases exponentially with height.

Below the pivot point, the pressure difference is equal to the difference between two exponentially increasing pressures. If the temperature is equal inside and outside, then the *relative* pressure difference is nearly constant with depth. This implies a nearly constant plasma β ($\beta = P_{gas}/P_{mag}$). The
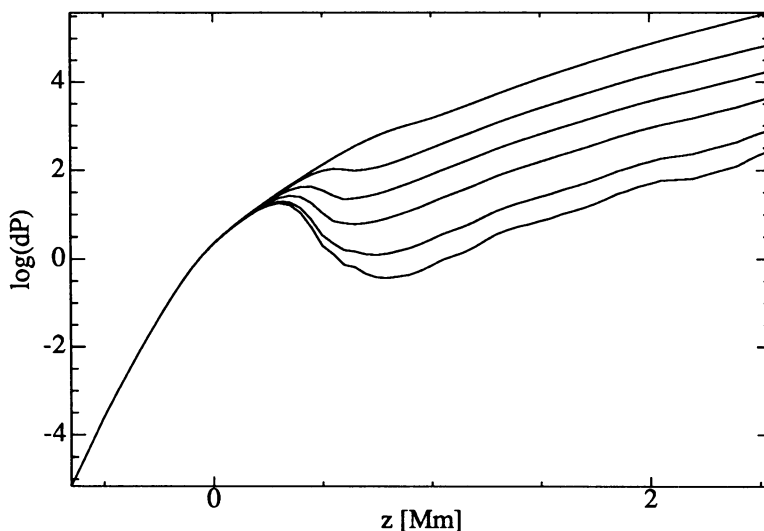
Figure 6. The pressure difference between the interior of the umbra and the external convection zone, after about two hours of simulated solar time. The six curves correspond to (from bottom to top) vertical displacements of the subsurface umbra, relative to the surrounding convection zone, of 10, 20, 50, 100, 200, and 500 *km*, respectively.

pressure difference may also be parametrized in terms of a relative displacement of the inside with respect to the outside.

Fig. 6 shows the gas pressure difference, as a function of height, for 6 different assumed height differences (10, 20, 50, 100, 200, and 500 *km*). Note the characteristic shape, with a pressure difference maximum near the pivot point. Only in the (unrealistic) case with a 500 *km* displacement is there no maximum near the pivot point. This is because, for this particular case, the internal gas pressure is a small fraction of the external pressure at all depths. We may conclude that, for reasonable values of the vertical displacement, the pressure difference has a characteristic shape, with a maximum near the pivot point.

When trying to fit the detailed distribution of field strength in sunspots, Jahn (1989) empirically deduced pressure difference profiles of just this shape. He also found it necessary to introduce volume currents in the penumbral region of his spot model, to satisfy constraints from measurements of penumbral magnetic fields.

3.3. SUNSPOT PARAMETERS

The pressure difference profile, together with the total magnetic flux of the spot, determines the umbra flux density, and hence the size and topology of

the spot. Since the shape of the pressure profile is nearly universal, the main characteristics of an idealized, symmetric, spot is determined uniquely by three parameters; the total flux, the depth of the pivot point (Wilson depression), and the (nearly constant) relative pressure difference in the subsurface layers. In principle, the subsurface entropy difference between the inside and the outside enters as a fourth independent parameter (van Ballegooijen, 1982), but small entropy differences do not significantly influence the structure near the surface.

The meaning of the first two parameters is clear, but what is the physical significance of the third one? Obviously, the relative pressure difference in the subsurface layers may be changed by pushing matter up or down the flux tube. In the Sun, this must be controlled by conditions in the deepest part of the flux rope, since that is where most of the mass in the flux rope is located. There may also be couplings to what happens in other part of a topologically connected structure. Globally, the total mass within a flux structure must be approximately conserved, if perhaps in a "leaky" way, depending on how coherent the flux structure is. In the most naive picture, pushing matter down at one place will push it up somewhere else.

When considering sunspots as part of the global solar magnetic field, such geometrical constraints have interesting implications that may be relevant for the behavior of active regions and for the solar dynamo process (cf. the next section). The relative pressure difference parameter might control the "looseness" of a spot or spot group, and might be what determines the systematic umbra intensity dependency on cycle phase discovered by Maltby and co-workers (Albregtsen & Maltby 1978, 1981; cf. also Maltby *et al.*, 1986). This is also the parameter who's evolution may be controlling the break-up of a spot. When the subsurface pressure difference decreases, the sub-surface field expands, and the spot may become unstable and break up.

The relative pressure difference at depth may also control the formation of spots and pores in an emerging flux region. Until the surface layers have cooled sufficiently, the surface pressure difference may not be large enough to hold a spot together at the surface, even if it is substantial some distance below the surface. An aggregate of flux is formed, with pores and faculae, loosely held together by the pressure difference at depth, but with insufficient pressure difference at the surface to form large spots. As the individual pores cool off, the surface pressure difference increases, and large spots form by merging of smaller pores and spots.

Morphological changes of the global magnetic field can change the relative pressure difference. If a flux structure is bent over backwards, because of differential rotation, it tends to become shorter along the bottom. Conservation of mass requires that matter be pushed up in the flux structure, so the sub-surface gas pressure difference drops. The surface flux concentration will no longer be held together below the surface, and spots will start to dissolve. This may be what happens in the following polarity of an active region, if the surface rotates more slowly than the bottom of the convection zone. Conversely, the leading part of a flux structure would be stretched out along the bottom, which would increase the sub-surface pressure difference, and hence tend to stabilize spots in the leading part of

active regions, as is observed.

The scenario works if the bottom of the convection zone rotates faster than the surface. Recent helioseismology measurements (e.g., Libbrecht, 1988) indicate that this is indeed the case, with the radially "stiff" mapping of the surface differential rotation through the top part of the convection zone turning over into more rigid rotation, near the lower boundary of the convection zone. Stenflo (1989ab) independenty deduced such a rotation profile by noting that rotation rates measured by correlating surface patterns over one or several rotation periods are systematically larger than the rotation rates for individual magnetic features, measured over shorter time periods, near the central meridian (Snodgrass, 1983).

4. Network and Facular Magnetic Fields

Network and facular magnetic fields consist of large numbers of small magnetic field structures, with magnetic field strengths of the order of 1 - 2 kG. Hence, their magnetic pressures are comparable to the photospheric gas pressure. They are similar to the larger pores and spots, but their sizes are typically smaller than can be resolved with present instruments. The local topology and time evolution of such structures are controlled by convection on the scale of granulation. The magnetic flux is concentrated in intergranular lanes. Their interiors become evacuated, because the surface radiative losses cannot be balanced by advection of entropy across the field lines. The flux concentrations are in quasi-static pressure equilibrium with surrounding evolving granules, and the flux concentrations "creep" into newly formed intergranular lanes. (Nordlund 1985d, 1986; Nordlund & Stein 1989)

Channeling of the radiative flux into thin flux structures may explain the brightness of small scale flux concentrations, as compared to darker larger scale flux concentrations such as pores and sunspots (Spruit 1976, Spruit & Zwaan 1981). The flux structures, which are perhaps better represented by slabs than by flux tubes, are separated from the surrounding granulation by a very thin boundary layer (Deinzer et al. 1984ab, Knölker et al. 1988, Grossmann-Doerth et al. 1988). Enhanced radiative heating and suppressed convective cooling of the upper photosphere may explain the relatively hot upper photospheric layers deduced from the temperature weakening of Stokes V profiles (Stenflo, 1975; Solanki & Stenflo 1984, 1985; Stenflo et al. 1987).

The topology and time evolution of larger clusters of small magnetic field concentrations is influenced by convection on larger scales: meso-granulation and super-granulation. Most of the field is swept to the boundaries of supergranulation cells, and local auto-correlation tracking of granules shows that the horizontal motion of small magnetic elements agrees with the horizontal motion of granules (Simon et al. 1988). The supergranular velocities are similar in the quiet sun and in the enhanced network (Wang 1989).

In plages, supergranulation cells are no longer visible, and horizontal velocities are significantly suppressed (Title et al. 1989). This may be related to a qualitative change of topology, where the magnetic field fills

TEMPERATURE   LOG DENSITY   MAGN. FIELD   VERT. VELOCITY

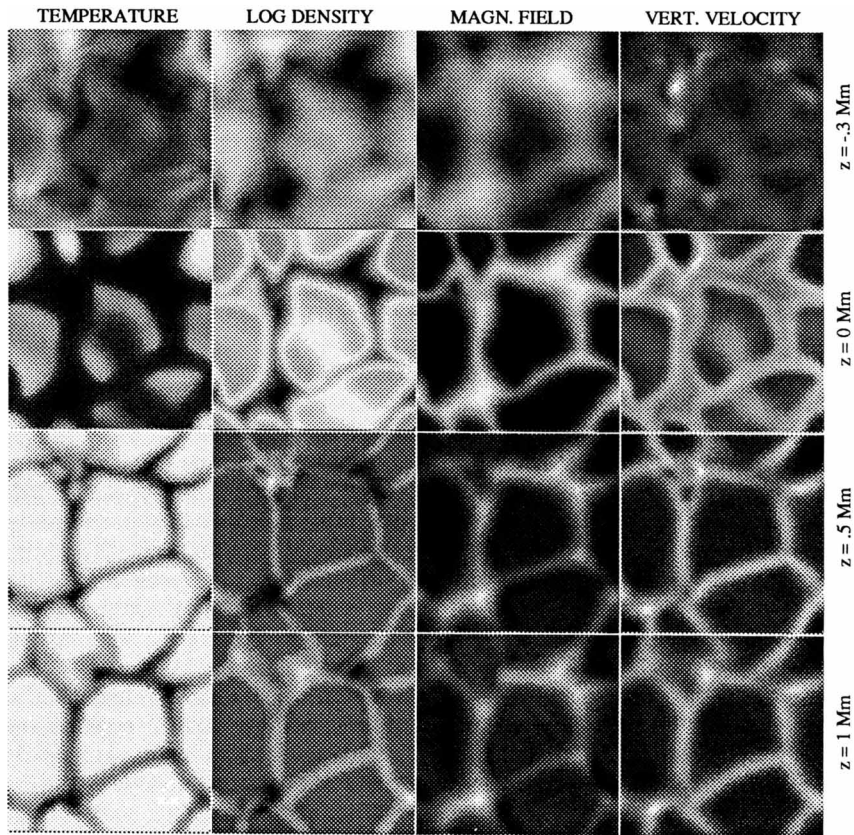z = -.3 Mm
z = 0 Mm
z = .5 Mm
z = 1 Mm

Figure 7. Composite plot, showing temperature, density, and the vertical components of the magnetic field and the velocity field, in horizontal planes at four different depths in a numerical model of the interaction of granulation and a (rather strong) facular magnetic field (Nordlund & Stein, 1989). The horizontal size of the model is 3×3 *Mm*.

essentially all available intergranular lanes, and hence becomes topologically connected in the horizontal plane (Nordlund & Stein, 1989). Such a magnetic flux topology inhibits large scale horizontal velocities, at least near the solar surface. The horizontal topology of a case with a 500 *G* average vertical field is illustrated in Fig. 7 (analogous to Fig. 1). Note that the surface (granulation) topology is visible over a larger range in depth, compared to the case in Fig. 1. Also, as illustrated by Fig. 1 of Nordlund & Stein (1989), the granules become more roundish, and their life times increase, relative to ordinary granules. This is because the nearly vertical sheets of magnetic field stabilize the convection patterns, by preventing the

interaction of flows from neighboring granules.

Schrijver (1989) has suggested a simple mechanism, based on the topology of the paths available for horizontal flux transport, to explain the rather sharp boundary between a plage and the surrounding network.   It may well be, however, that plages are intrinsically coherent.   If they are the surface manifestations of subsurface flux ropes with a relative gas pressure difference sufficient to hold the flux together at depth, but insufficient to bring the flux together into sunspots, then the relatively well defined boundary may simply reflect the boundary of the subsurface flux rope.   Near the surface, the flux rope is "frayed", with the individual strands concentrated to kilo Gauss strength by the surface effects discussed above. However, below the surface, the flux rope may retain some of the coherent structure it undoubtedly had when emerging through the surface as the following polarity part of an emerging flux region.

5.   Active Regions and the Solar Dynamo

Active regions are often considered passive consequences of the solar dynamo; the queer and intricate surface manifestation of subsurface dynamo action.   However, a scenario for a "topological solar dynamo" may be constructed where active region magnetic fields play an important part in the dynamo process, and the detailed connectivity of the global solar magnetic field is essential to the dynamo process (Nordlund, 1989).   The "topological dynamo" is a classical "$\alpha - \omega$ dynamo", but complemented with detailed suggestions for the topology of the α and ω parts of the process.   This scenario is able to explain a number of observed features of the solar cycle and solar active regions.   A short summary of the main features is given here:

A flux rope breaking off from an azimuthal magnetic flux system at the bottom of the convection zone, and rising towards the surface, experiences a systematic coriolis force due to the persistent expansion of ascending plasma. The sense of the coriolis force is contrary to the sense of rotation; i.e., the rising part of the flux rope tends to rotate its leading polarity towards the equator and its following polarity away from the equator.   This tendency is counteracted by the tension force along the flux rope, which tends to keep the flux rope in alignment with the main azimuthal flux system.   The well known tendency for active region magnetic fields to have a slight inclination to the equator is most likely a consequence of this effect which, of course, is nothing else than what is usually called the "α-effect" in dynamo theory. In general terms, the α-effect is responsible for generating a poloidal component of the magnetic field, from an originally azimuthal field component.

The other ingredience in a classical $\alpha - \omega$ dynamo is the "ω-effect", which regenerates an azimuthal component, of opposite sign to the original one, from the poloidal component.   In general terms, the ω effect is of course a consequence of the differential rotation of the solar convection zone, acting on the poloidal component of the global solar magnetic field.   Note, however,

that the "poloidal" part generated by the weak tilt of active region magnetic fields is localized to the active region. Part of the "topological dynamo" scenario is a suggestion for the actual topology of the "ω-effect", which involves the distortion of active region magnetic fields by differential rotation.

As an active region flux rope breaks through the surface, the crest of the loop extends into the corona. We know observationally that reconnection is efficient in the corona. On the time scale of days, the original connectivity between leading and following polarity is lost. We may therefore regard the original flux rope as effectively severed above the surface, with the following and leading polarity crossections acting as two "loose" ends of the original flux rope.

As discussed in the previous section, the leading polarity end of the flux rope, with flux concentrated into a few spots, is "dragged" along by the faster rotation at depth. The following polarity end is bent over backwards by the differential rotation, and forms a diffuse (plage) crossection with the surface. As a consequence, the latitudinal position of the leading polarity remains well defined and stable, while the following polarity, because it is bent over backwards, more easily drifts in latitude. The observed poleward drift of the following polarity implies that the dispersed plage area hauls the bottom field along as a heavy rope trailing polewards around along the bottom. This leads to "unwinding" of the bottom part of the following polarity from the original azimuthal flux system, and the winding up of new azimuthal flux in the opposite direction at high latitudes. At the same time, the leading flux is being wound up on the equatorward side of the azimuthal flux system, which leads to an equatorward migration of the original azimuthal flux system. This process keeps going as long as the surface rotates slower than the bottom of the convection zone. When the original azimuthal flux system reaches latitudes where the radial differential rotation vanishes (cf. Libbrecht 1988, Fig. 2), the "unwinding" process wins over the "winding" process, and the original azimuthal flux system eventually vanishes. In the mean time, a new flux system with opposite polarity has formed at high latitudes, and a new cycle begins.

6. Concluding Remarks

We have stressed, throughout this paper, the importance of considering the three-dimensional topology of solar magnetic fields and flows. Because of the enormous pressures and densities in the deep convection zone, relative to the observable surface, much of the large scale and long time behavior of surface phenomena is likely to be controlled from below. The near adiabatic and anelastic nature of subsurface flows, and the connectivity of magnetic fields, provide important constraints on the behavior of the subsurface flows and magnetic fields. We can only observe the surface manifestations of these subsurface phenomena, and we must deduce the behavior below the surface by indirect means.

As we have illustrated here, numerical simulations may play an important

role in this process, by providing examples of the complicated behavior, and of the three-dimensional topologies involved. Numerical simulations are most useful when set up to directly model the behavior of solar phenomena, by using three-dimensional and unbounded geometries, by accurately modeling surface radiative transfer effects, and by using realistic equations of state and absorption coefficients. One argument for this detailed approach is to be able to directly compare with observed surface phenomena. Another important reason for using a realistic simulation is to avoid introducing spurious effects, e.g., at non-penetrative or reflecting boundaries.

However, given results of such detailed and realistic simulations, qualitative interpretation of the often very complicated spatial and temporal behavior is vitally important, in order to identify the essential physical processes, and to be able to draw more general conclusions from the numerical models, which are necessarily limited in temporal and spatial extent and resolution.

Solar physics is presently enjoying a renaissance, with new instruments and clever observational techniques, together with supercomputer numerical simulations, providing the impetus for rapid progress in our understanding of physical processes on the Sun. The development of new earth- and space-based instrumentation (LEST, SOHO, OSL), and the continual improvement of computer hardware and software, will supply even more powerful tools to assist our venture.

Acknowledgements

REFERENCES

Albregtsen, F., Maltby., P., 1978, *Nature*, **274**, 41.
Albregtsen, F., Maltby., P., 1981, *Solar Phys.* **71**, 269.
Bray, R.J., Loughhead, R.E., Durrant, C.J., 1984, *The Solar Granulation*, Cambridge University Press.
Deinzer, W., Hensler, G., Schüssler, M., Weisshaar, E., 1984a, *Astron. Astrophys.* **139**, 426.
Deinzer, W., Hensler, G., Schüssler, M., Weisshaar, E., 1984b, *Astron. Astrophys.* **139**, 435.
Gilman, P.A., Miller, J., 1986, *Astrophys. J. Suppl.* **61**, 585
Glatzmaier, G.A., 1987, in *The Solar Internal Angular Velocity: Theory, Observations and Relationships to the Solar Magnetic Fields,* eds. B.R. Durney and S. Sofia, Reidel, Dordrecht, p. 263.

Grossmann-Doerth, U., Schüssler, M., Solanki, S.K., 1988, *Astron. Astrophys.* **206**, L37.

Hurlburt, N. E., Toomre, J. and Massaguer, J. M. 1984, *Astrophys. J.* **282**, 557.

Jahn, K., 1989, *Astron. Astrophys.* (in press).

Knölker, M., Schüssler, M., Weisshaar, E., 1988, *Astron. Astrophys.* **194**, 257.

Leighton, R.B., Noyes, R.W., and Simon, G.W., 1962, *Astrophys. J.* **135**, 474.

Libbrecht, K.G., 1988, *Proc. Symp. Seismology of the Sun and Sun-like Stars, Tenerif, Spain, 26-30 September 1988*, ESA SP-**286**, p. 131.

Lites, B.W., Nordlund, Å., and Scharmer, G.B. 1989, in *Proceedings NATO Advanced workshop on Solar and Stellar Granulation*, eds. R.J. Rutten and G. Severino, Kluwer Academic Publishers, Dordrecht, p. 349.

Maltby, P., Avrett, E.H., Carlsson, M., Kjeldseth-Moe, O., Kurucz, R.L., Loeser, R., 1986, *Astrophys. J.* **306**, 284.

Müller, R., 1989, in *Proceedings NATO Advanced workshop on Solar and Stellar Granulation*, eds. R.J. Rutten and G. Severino, Kluwer Academic Publishers, Dordrecht, p. 9.

Nordlund, Å., 1982, *Astron. Astrophys.* **107**, 1.

Nordlund, Å, 1983, in "Solar and Stellar Magnetic Fields: Origin and Coronal Effects", ed. J.-O. Stenflo, *IAU Symp.* **102**, 79.

Nordlund, Å, 1984a, in *Small Scale Processes in Quiet Stellar Atmospheres*, ed. S.L. Keil, Sacramento Peak Observatory, Sunspot, N.M. 88349, p. 174.

Nordlund, Å, 1984b, in *Small Scale Processes in Quiet Stellar Atmospheres*, ed. S.L. Keil, Sacramento Peak Observatory, Sunspot, N.M. 88349, p. 181.

Nordlund, Å, 1984c, in *The Hydromagnetics of the Sun, Proc. 4th European Meeting in Solar Physics*, ESA SP-**220**, p. 37.

Nordlund, Å, 1985a, *Solar Phys.* **100**, 209.

Nordlund, Å, 1985a, in *Problems in Stellar Spectral Line Formation Theory*, eds. J.O. Beckman and L. Crivellari, Reidel, Dordrecht, p. 215.

Nordlund, Å, 1985c, in *Proc. MPA/LPARL Workshop on Theoretical Problems in Solar Physics*, MPA **212**, p. 1.

Nordlund, Å, 1985d, in *Proc. MPA/LPARL Workshop on Theoretical Problems in Solar Physics*, MPA **212**, p. 101.

Nordlund, Å, 1986, *Abh. der Akad. der Wissensch. in Göttingen*, **38**, 83.

Nordlund, Å, 1989, (in preparation).

Nordlund, Å. and Dravins, D., 1989, *Astron. Astrophys.* (in press).

Nordlund, Å., Stein, R.F., 1989a, *Proceedings NATO Advanced workshop on Solar and Stellar Granulation*, eds. R.J. Rutten and G. Severino, Kluwer Academic Publishers, Dordrecht, p. 453.

November, L.J., Toomre, J, and Gebbie, K.B., 1981, *Astrophys. J.* **245**, L123.

November, L.J., Simon, G.W., 1988, *Astrophys. J.* **333**, 427.

Scherrer, P.H., Hoeksema, J.T., Bogart, R.S., Walker, Jr., A.B.C., Title, A.M., Tarbell, T.D., Wolfson, C.J., Brown, T.M., Christensen-Dalsgaard, J., Gough, D.O., Kuhn, J.R., Leibacher, J.W., Libbrecht, K.G., Noyes, R.W., Rhodes, Jr., E.J., Toomre, J., Zweibel, E.G., Ulrich Jr., R.K., 1989, ESA SP-**1104**, p. 25.

Schrijver, C.J., 1989, *Solar Phys.* (in press).

Simon, G.W., and Leighton, R.B., 1964, *Astrophys. J.* **140**, 1120.

Simon, G.W., Title, A.M., Topka, K.P., Tarbell, T.D., Shine, R.A., Ferguson, S.H., Zirin, H., and the Soup team, 1988, *Astrophys. J.* **327**, 964.

Snodgrass, H.B., 1983, *Astrophys. J.* **270**, 288.

Solanki, S.K., Stenflo, J.O., 1984, *Astron. Astrophys.* **140**, 185.

Solanki, S.K., Stenflo, J.O., 1985, *Astron. Astrophys.* **148**, 123.

Spruit, H.C., 1976, *Solar Phys.* **50**, 269.

Spruit, H.C., Zwaan, C., 1981, *Solar Phys.* **70**, 207.

Stenflo, J.O., 1975, *Solar Phys.* **42**, 79.

Stenflo, J.O., 1989a, *Astron. Astrophys.* **210**, 403.

Stenflo, J.O., 1989b, *Astron. Astrophys. Review* **1**, 3.

Stenflo, J.O., Solanki, S.K., Harvey, J.W., 1987, *Astron. Astrophys.* **171**, 305.
Stein, R.F. and Nordlund, Å, 1989, *Astrophys. J. (Letters)* **342**, L95.

Title, A.M., Tarbell, T.D., Topka, K.P., Ferguson, S.H., Shine, R.A., and the SOUP team, 1989, *Astrophys. J.* **336**, 475.

van Ballegooijen, A.A., 1982, *Astron. Astrophys.* **106**, 43.

Wang, H., 1989, *Solar Phys.* (in press).

Zirin, H., 1987, *Solar Phys.* **114**, 239.